

Synthesis of NiTi intermetallics by self-propagating combustion

C.L. Yeh*, W.Y. Sung

Department of Mechanical and Automation Engineering, Da-Yeh University, 112 Shan-Jiau Road, Da-Tsuen, Changhua 51505, Taiwan

Received 6 November 2003; received in revised form 10 December 2003; accepted 10 December 2003

Abstract

The production of NiTi intermetallic compounds from elemental powder compacts was conducted by self-propagating high-temperature synthesis (SHS) in this study. Effects of initial sample density, preheating temperature, and Ni particle size on the combustion characteristics, as well as on the final composition and morphology of products were studied. For the samples with densities between 50 and 60% theoretical maximum density (TMD) under preheating temperatures in the range of 100–300 °C, the synthesis process showed two consecutive combustion stages, including the propagation of combustion front and the subsequent bulk combustion. Under these conditions, high-density products containing NiTi as the major phase with small amounts of secondary phases of NiTi₂ and Ni₃Ti were obtained. However, porous combustion products with a significant amount of unreacted Ni were produced from the 45% TMD samples under preheating temperatures of 100 and 150 °C, due to the lack of the second combustion stage. The amount of unreacted Ni in the final composition was greatly reduced by increasing the initial sample density and preheating temperature, or by using smaller Ni particles in the samples. In addition, the use of smaller Ni particles also led to an increase in the product density up to about 95% relative to the density of NiTi intermetallic.

© 2004 Elsevier B.V. All rights reserved.

Keywords: Intermetallics; Chemical synthesis; X-ray diffraction

1. Introduction

The NiTi intermetallics have received increasing attention because of their excellent mechanical properties, unique shape memory effect and superelasticity, good corrosion resistance, superior damping capability, and high biocompatibility [1–5]. They have been practically used for couplings, actuators, smart materials, as well as external and internal biomedical applications, e.g. orthodontic arch wires, catheters, orthopaedic implants, and in cardiovascular surgery, etc. [1–5]. In addition, the porous NiTi alloy shows promising potential in the application of bone implantation because the porous structure allows the ingrowth of new bone tissue along with the transport of body fluids, thus ensuring a harmonious bond between the implant and the body [6,7].

Conventionally, NiTi intermetallics are produced by arc or induction melting followed by hot working and forming. Arc melting requires multiple re-melts to achieve sufficient homogeneity, while induction melting has the drawback of

oxygen contamination [2]. The powder metallurgy technique has also been used for the NiTi fabrication and offers the ability to avoid the problems of casting defects due to segregation and to produce a variety of component shapes while minimizing subsequent machining operations [8]. However, the high-density NiTi product is difficult to obtain by the powder metallurgy. Recently, Locci et al. [9] synthesized dense NiTi intermetallics from elemental powder compacts using the electric field activation technique with simultaneous compression. It was found that the amounts of secondary phases (including Ni₃Ti, NiTi₂, and Ni₄Ti₃) in the products were decreased by either increasing the current density and the synthesis time, or decreasing the particle size of reactant powders. Under the condition with a current in the range of 1300–1500 A, a dense product (99% relative density) consisting of NiTi as the major phase and a small amount of NiTi₂ was obtained in a relatively short processing time of 20 min [9].

In addition to the techniques mentioned above, combustion synthesis with the advantages of time and energy savings has been recognized as an attractive alternative to the conventional methods of producing advanced materials, including carbides, borides, nitrides, hydrides, and intermetallics, etc. [10,11]. Combustion synthesis of NiTi intermetallics can

* Corresponding author. Tel.: +886-4-8511888x2118; fax: +886-4-8511215.

E-mail address: clyeh@mail.dyu.edu.tw (C.L. Yeh).

be conducted in either of two modes, the self-propagating high-temperature synthesis (SHS) [6,7] and the thermal explosion [12–14]. Due to the relatively low exothermic characteristic of the reaction between Ni and Ti, preheating the sample prior to the ignition is necessary to achieve self-sustained combustion [6,12]. By using combustion synthesis in SHS mode with preheated samples, highly porous NiTi alloys with a porosity of about 60 vol.% were obtained by Li et al. [6]. The preheating temperature was shown to have a significant effect on the microstructure of the products and the anisotropy of the pore structure was attributed to the formation of liquid phase during the SHS process [6]. In the thermal explosion mode of combustion synthesis conducted by Yi and Moore [12], the combustion temperature was found to be much higher than the melting point of NiTi alloy so that cast products were obtained. Moreover, the amount of the NiTi phase in final products increased as the heating rate to ignition temperature was increased in the thermal explosion synthesis [14].

The objective of the present study was to experimentally investigate the synthesis of NiTi intermetallic compounds by SHS using compacted samples from elemental powders. Effects of initial sample density, preheating temperature, and particle size of reactant powders on the final composition and morphology of combustion products were studied. The dynamics of combustion wave, i.e., flame-front trajectory and propagation velocity, as well as the combustion temperature were measured. In particular, a close study was made of combustion characteristics, including the propagation of self-sustained combustion front, the melting of powder compacts, and the subsequent bulk reaction.

2. Experimental methods of approach

Two types of nickel (Ni) powders with different particle sizes of 325 mesh ($<45\ \mu\text{m}$, Acros Organics, 99.9% purity) and 3–7 μm (Strem Chemicals, 99.9% purity) were mixed with titanium (Ti) powders (Strem Chemicals, 325 mesh, and 99% purity) to form sample compacts. Ni and Ti powders at equiatomic stoichiometry were dry mixed in a ball mill for 10 h. The XRD pattern of blended mixtures exhibited no peaks other than those of the starting elements, with an indication that no mechanical alloying of the powders occurred during the milling operation. The mixed powders were then cold-pressed into cylindrical samples with a diameter of 7 mm and a height of 12 mm. In order to obtain test samples with different porosities, the powder compacts with Ni particles of 325 mesh were formed with the initial packing densities equal to 45, 50, 55, and 60% of the theoretical maximum density (TMD) of the powder mixture. The samples using Ni powders of 3–7 μm were prepared at 60% TMD.

The SHS experiments were conducted in a stainless-steel windowed combustion chamber, as shown in Fig. 1, under an atmosphere of high purity argon (99.99%). On account of the low combustion heat between titanium and nickel, the sample holder was equipped with a 600 W cartridge heater to preheat the test sample prior to the ignition. The ignition was accomplished by a heated tungsten coil with a voltage of 60 V and a current of 1.5 A.

The propagation rate of the combustion wave was measured by recording the whole combustion event with a color CCD video camera (Pulnix TMC-7) at 30 frames per second.

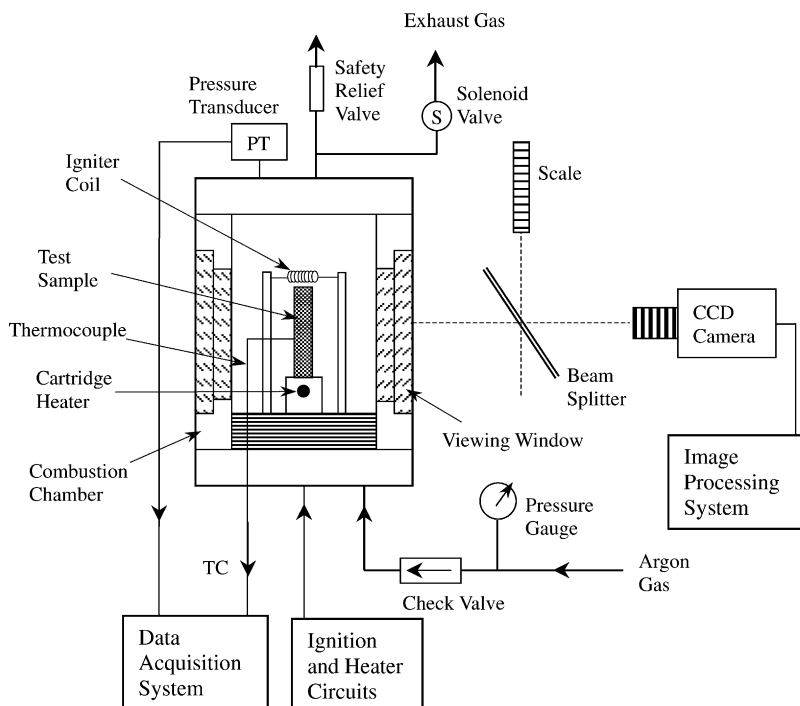


Fig. 1. Schematic diagram of experimental setup to synthesize NiTi intermetallic compounds by SHS.

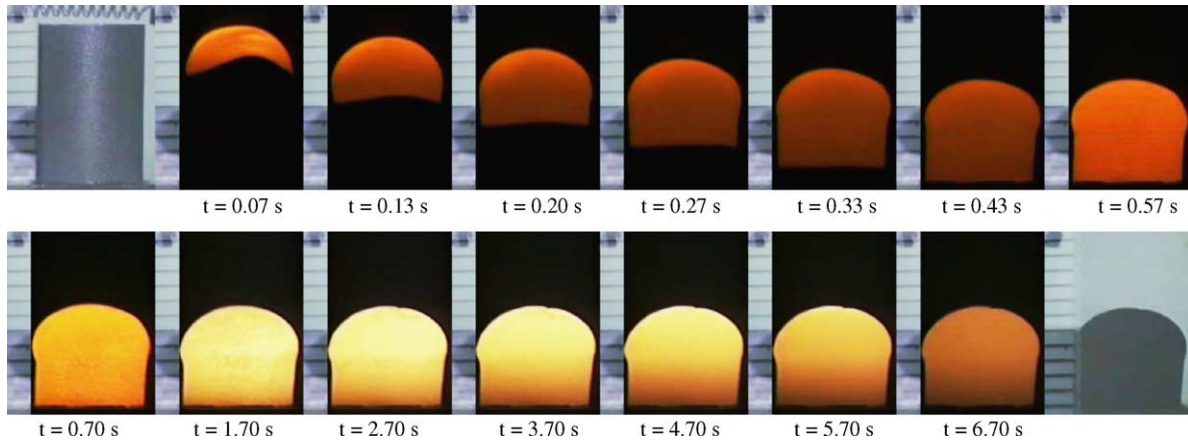


Fig. 2. Recorded combustion images of SHS process associated with a 55% TMD sample at $T_p = 300^\circ\text{C}$ to form a dense product.

The exposure time of each recorded image was set at 0.1 ms. To facilitate the accurate measurement of instantaneous locations of the combustion front, a beam splitter (Rolyn Optics), with a mirror characteristic of 75% transmission and 25% reflection, was used to optically superimpose a scale onto the image of the test sample. The combustion temperature of powder compact was measured by a fine-wire (125 μm) Pt/Pt-13%Rh thermocouple (Omega Inc.) attached on the sample surface.

The density of end products was determined by geometrical measurements and the Archimedes method. The microstructure of combustion products was examined under a scanning electron microscope (SEM). The chemical composition was identified by an X-ray diffractometer with Cu $K\alpha$ radiation operating at 40 kV.

3. Results and discussion

3.1. Observation of combustion characteristics

Experimental observations indicate that the combustion characteristics associated with the formation of NiTi inter-

metallics by SHS depend on both the initial sample density and the preheating temperature (T_p). The typical combustion process of a Ni/Ti powder compact in this study is presented in Fig. 2. As shown in Fig. 2, upon the ignition a distinct and self-sustained flame-front propagates downward with a nearly constant velocity. It is obvious that the propagation of the flame-front is accompanied by a significant melting of the sample. Fig. 2 also shows that the flame-front rapidly reaches the bottom of the sample at about $t = 0.43$ s and transforms the cold reactant into a hot product. Beyond the flame-propagation stage, the luminosity on the sample gradually increases rather than fading away. As shown in Fig. 2, the sample is highly incandescent for a relatively long period of time from $t = 0.7$ to 4.7 s. This observation suggests that the reaction process consists of two consecutive combustion stages. The first stage corresponds to the propagation of the self-sustained flame-front, where the reaction takes place. The second stage signifies a prolonged bulk combustion period, within which vigorous reactions occur. Based upon the above observations, it was believed that some molten liquid was formed at the combustion front during the flame-propagation stage, resulting in the shrinkage of the sample. Subsequently, the spreading of the liquid

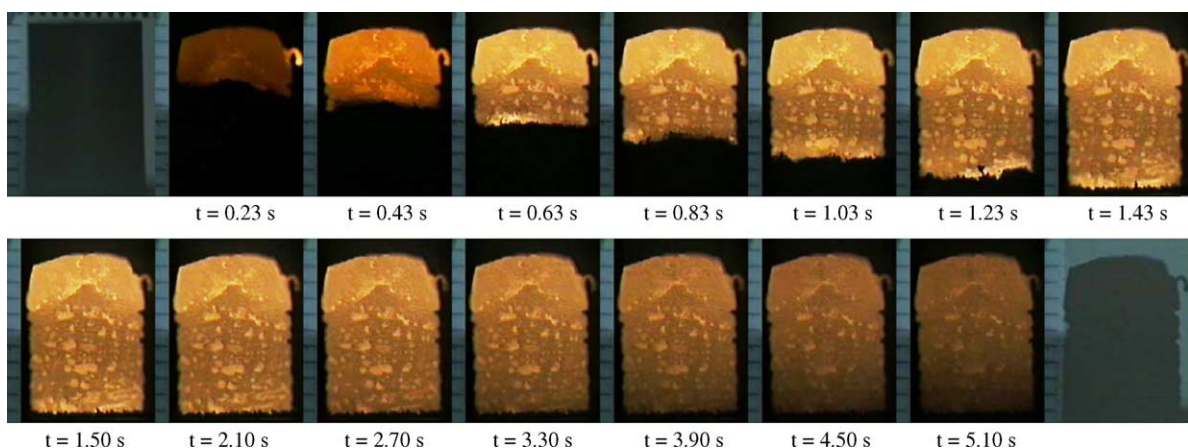


Fig. 3. Recorded combustion images of SHS process associated with a 45% TMD sample at $T_p = 100^\circ\text{C}$ to form a porous product.

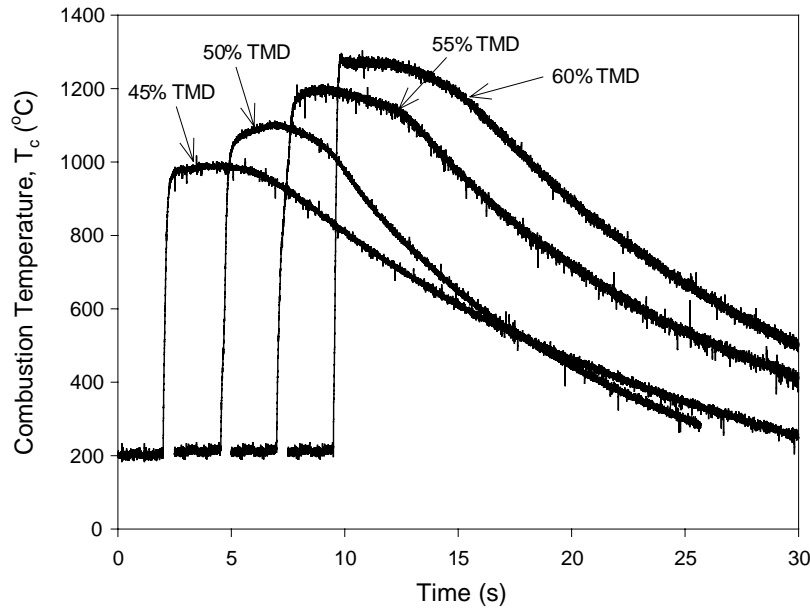


Fig. 4. Effect of initial sample density on combustion temperature of sample compacts at $T_p = 200^\circ\text{C}$.

within the porous sample enhanced both heat and mass transfer, thus leading to the second combustion stage. In this study, the test sample with an initial density between 50 and 60% TMD and under a preheating temperature ranging from 100 to 300°C experienced two combustion stages similar to those shown in Fig. 2. Due to the substantial melting during the first combustion stage, high-density final products were obtained. It is useful to note that in this study the ignition cannot be achieved under the preheating temperature lower than 100°C .

In contrast, as shown in Fig. 3, the SHS process of a 45% TMD sample under a preheating temperature of 100°C exhibits only the first combustion stage. That is, after the passage of the self-sustained flame-front, the luminosity on the sample slowly vanished and the second combustion stage was absent. Moreover, the sample almost retained its original shape with no deformation except for the top portion, where the ignition took place. As a result, a porous end product was obtained. In this study, only the 45% TMD samples preheated at 100 or 150°C were subjected to this type of

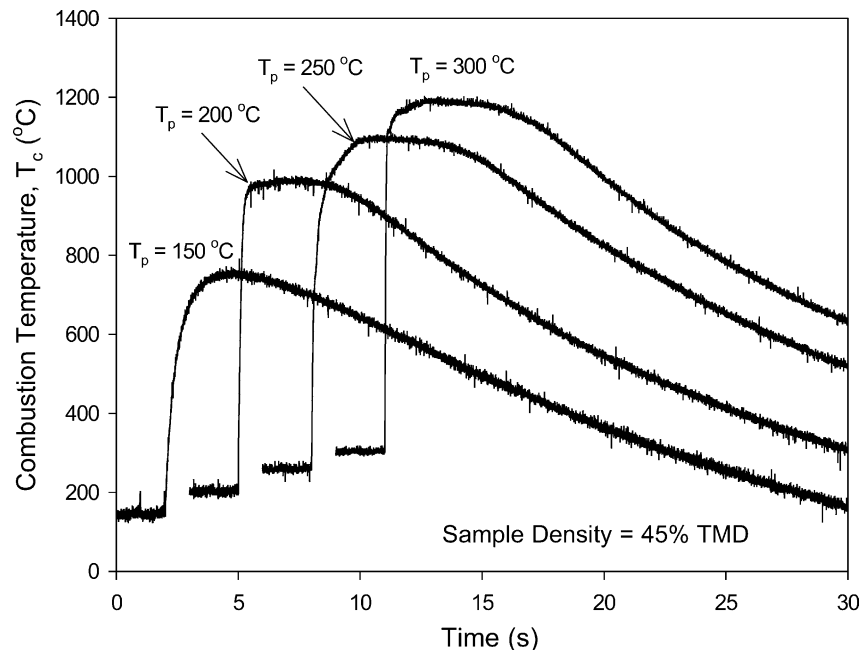


Fig. 5. Effect of preheating temperature on combustion temperature of 45% TMD sample compacts.

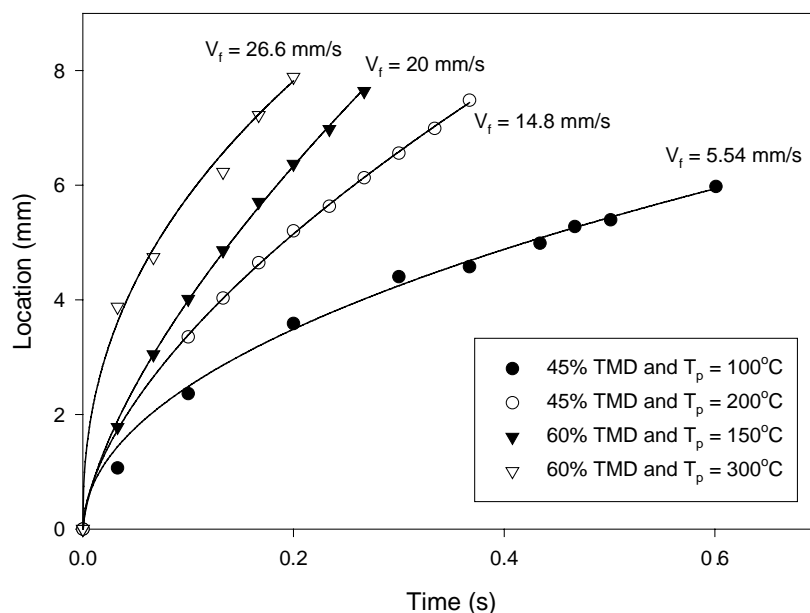


Fig. 6. Flame-front trajectories of sample compacts under different test conditions.

the combustion process. This might be caused by the fact that the combustion temperature was too low to produce any liquid phase; therefore, the reaction occurred mainly in the solid phase [6].

3.2. Measurement of combustion temperature

Fig. 4 shows the effect of initial sample density on measured temperature profiles of sample compacts at a constant preheating temperature of 200 °C. The temperature profile is characteristic of an abrupt increase representing the ar-

rival of the flame-front. Immediately following the abrupt rise, the profile reveals a relatively flat plateau region almost at the highest temperature for about 4 to 5 s, beyond which a gradual decline in temperature occurs. This plateau region represents the prolonged bulk combustion stage after the passage of the flame-front, as described in Fig. 2. It is also found in Fig. 4 that the combustion temperature increases with increasing initial sample density, since the higher the initial sample density, the better the heat transfer from the burned to the unburned region. In addition, the highest combustion temperatures of all four samples

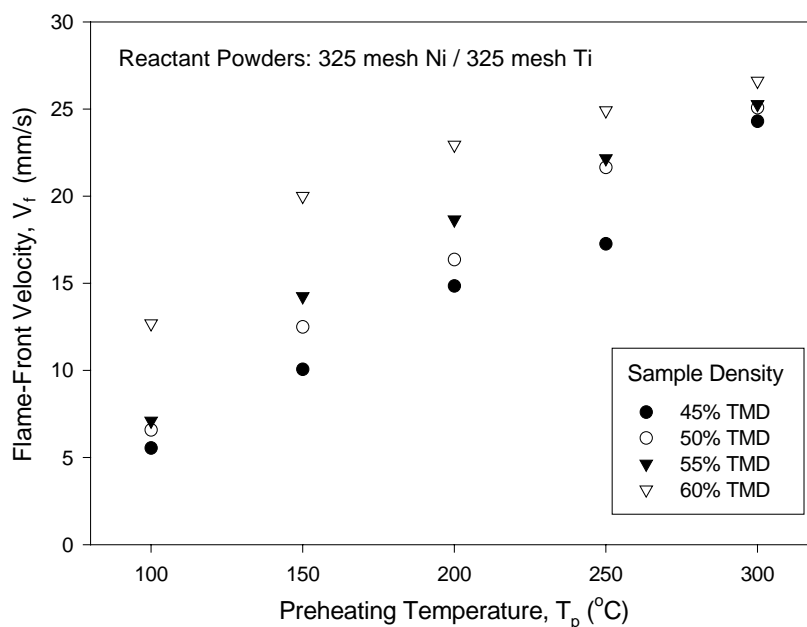


Fig. 7. Effects of preheating temperature and sample density on flame-front propagation velocity.

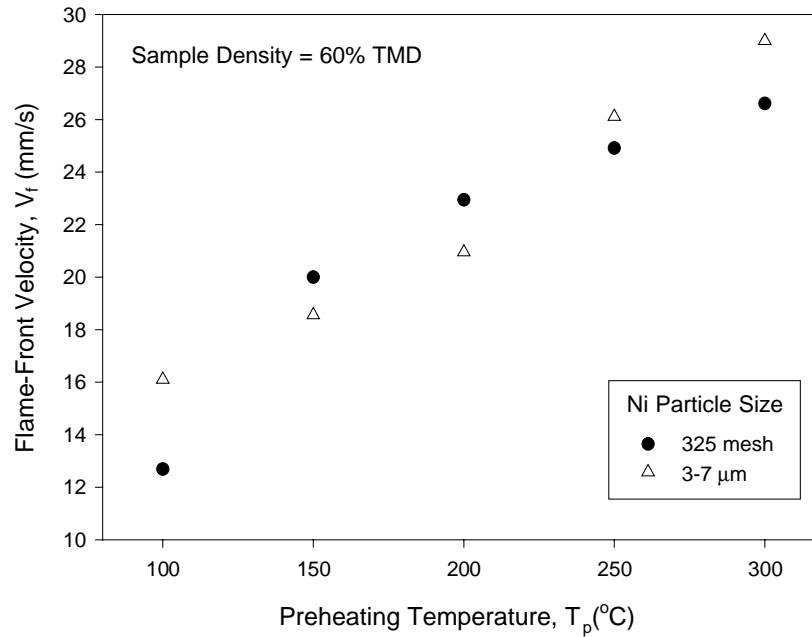


Fig. 8. Effect of particle size of Ni powders on flame-front propagation velocity.

shown in Fig. 4 are above the lowest eutectic temperature (942 °C) of the Ni/Ti mixture, but below the melting point of the NiTi alloy (1310 °C). This implies the formation of the eutectic liquid at the combustion front and during the subsequent bulk combustion stage.

Fig. 5 indicates that an increase in sample preheating temperature leads to an increase in combustion temperature. It is important to point out from Fig. 5 that at a preheating temperature of 150 °C the maximum combustion temperature of the 45% TMD powder compact reaches

only about 770 °C. This is lower than the eutectic temperature of 942 °C, indicating that there is no formation of any liquid phase during the self-sustained combustion stage. This result further explains the synthesis of porous final products from the 45% TMD compacts at $T_p = 100$ and 150 °C. As shown in Fig. 5, however, combustion temperatures are found to be higher than the lowest eutectic temperature under preheating temperatures of 200 °C and above, thus resulting in the formation of dense final products.

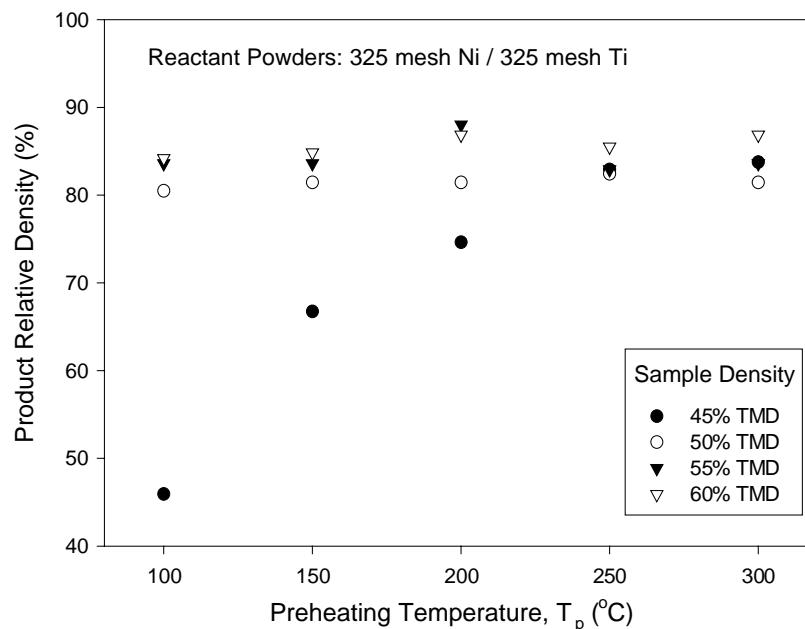


Fig. 9. Effects of preheating temperature and sample density on relative density of final products.

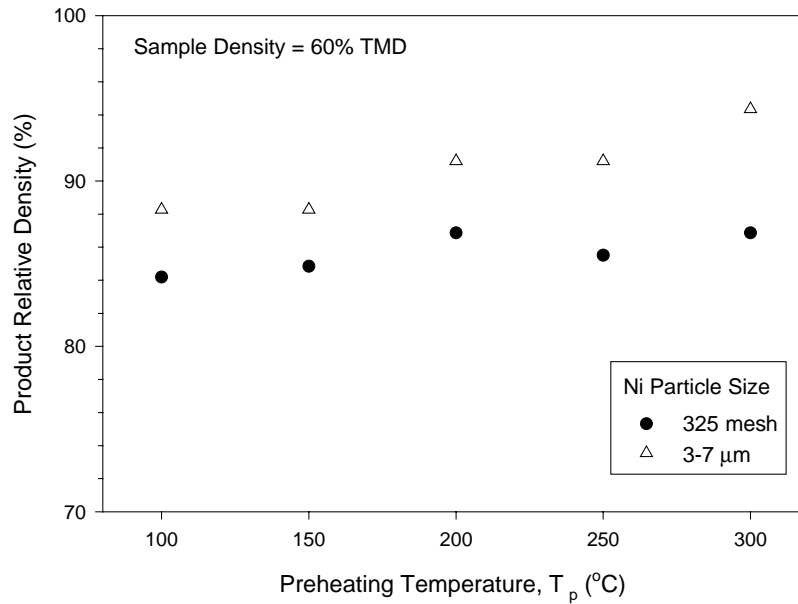


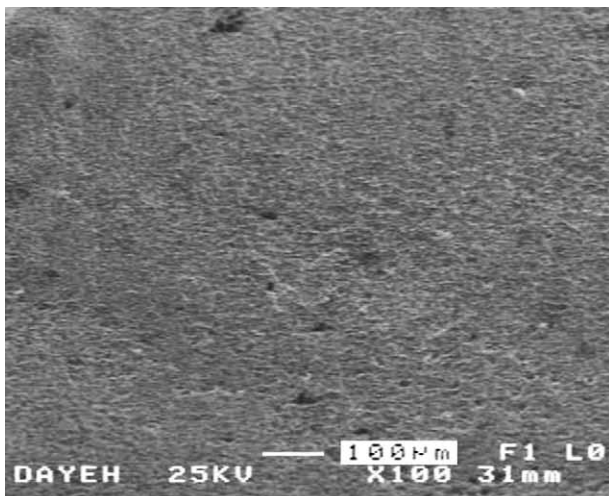
Fig. 10. Effect of particle size of Ni powders on relative density of final products.

3.3. Measurement of flame-front trajectory and propagation velocity

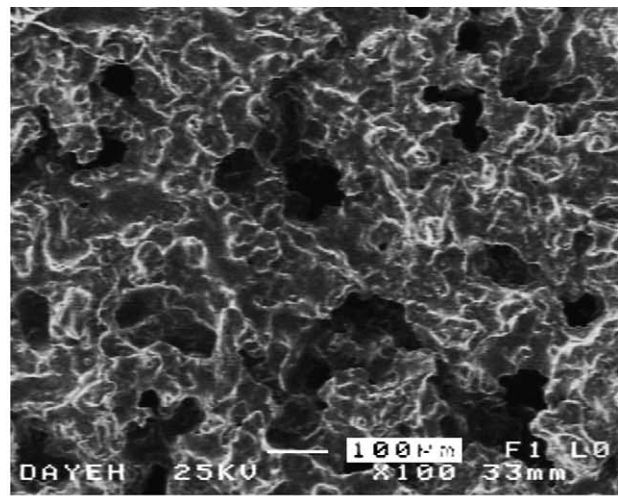
The flame-front propagation velocity (V_f) was determined in this study from the measured flame-front trajectory, which was constructed upon the recorded film images. Fig. 6 shows a plot of flame-front trajectories of samples under different test conditions. The trajectory indicates that the flame-front velocity is relatively high right after the ignition and then experiences a noticeable deceleration, finally arriving at a nearly constant value. The high propagation velocity in the early stage was mainly attributed to the external heat flux from the igniter, and the later phase featuring a

constant velocity represented the self-sustained propagation of flame-front. The values of V_f marked in Fig. 6 stand for the front velocity in the self-sustained combustion zone.

Fig. 7 shows that the flame-front propagation velocity increases significantly with an increase in the sample preheating temperature. In addition, the increase of sample density also causes the increase of flame-front velocity. These results were mainly due to the increase of combustion temperature with preheating temperature and sample density. However, as shown in Fig. 8, the front-front propagation velocity is not affected by the Ni particle size used in sample compacts at 60% TMD, largely because of the formation of the eutectic liquid during the propagation of the flame-front.



(a)



(b)

Fig. 11. SEM micrographs showing microstructures of (a) a dense product synthesized from a 55% TMD sample at $T_p = 300^\circ\text{C}$, and (b) a porous product synthesized from a 45% TMD product at $T_p = 100^\circ\text{C}$.

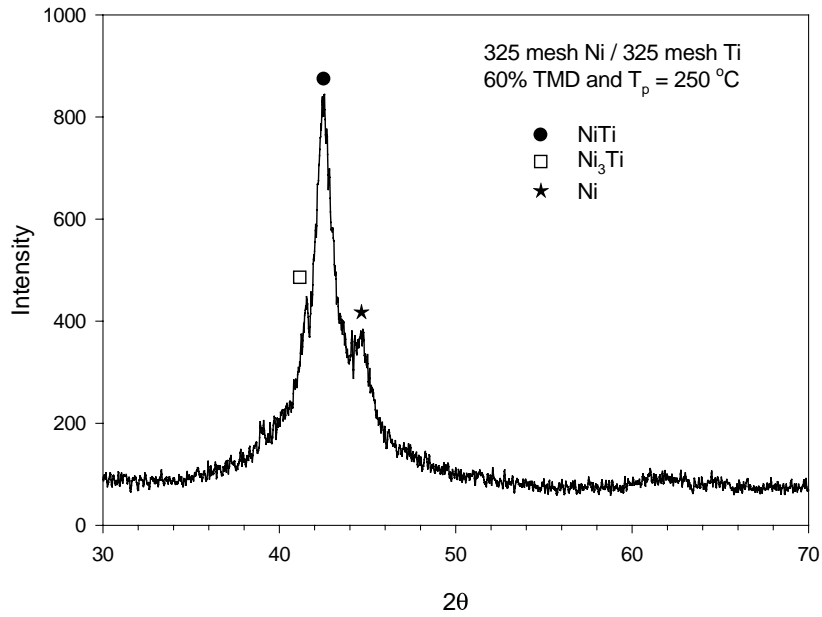


Fig. 12. XRD spectrum of product obtained from a 60% TMD sample compact using 325 mesh Ni powders at $T_p = 300^\circ\text{C}$.

3.4. Analysis of morphology and composition of combustion products

The densities of end products obtained from sample compacts with 325 mesh Ni powders are presented in Fig. 9 as a function of preheating temperature and initial sample density. It is evident that, except for the 45% TMD samples, the densities of combustion products are nearly independent of the preheating temperature. For the 50, 55, and 60% TMD samples, the densities of final products, in general, increased slightly with an increase in the initial sam-

ple density and were ranged between 80 and 90% of the density of NiTi alloy. For the 45% TMD sample, it was found that the product density increased substantially with the preheating temperatures from 100 to 250°C . This was caused by the fact that the 45% TMD samples yielded porous end products under $T_p = 100$ and 150°C , and produced dense compounds with further increase in the preheating temperature.

Fig. 10 shows that the use of smaller Ni powders as the starting reactant contributes to an increase in the density of final products. Combustion product with about 95%

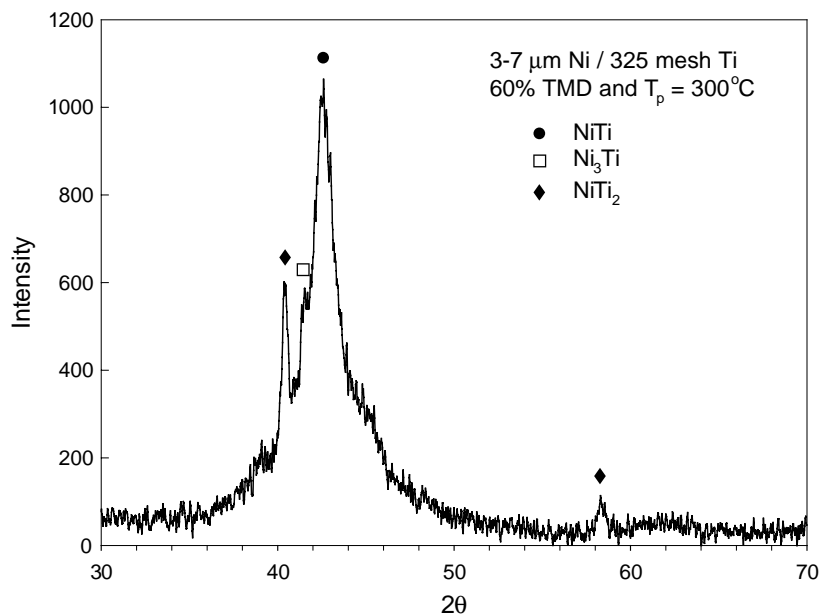


Fig. 13. XRD spectrum of product obtained from a 60% TMD sample compact using 3–7 μm Ni powders at $T_p = 300^\circ\text{C}$.

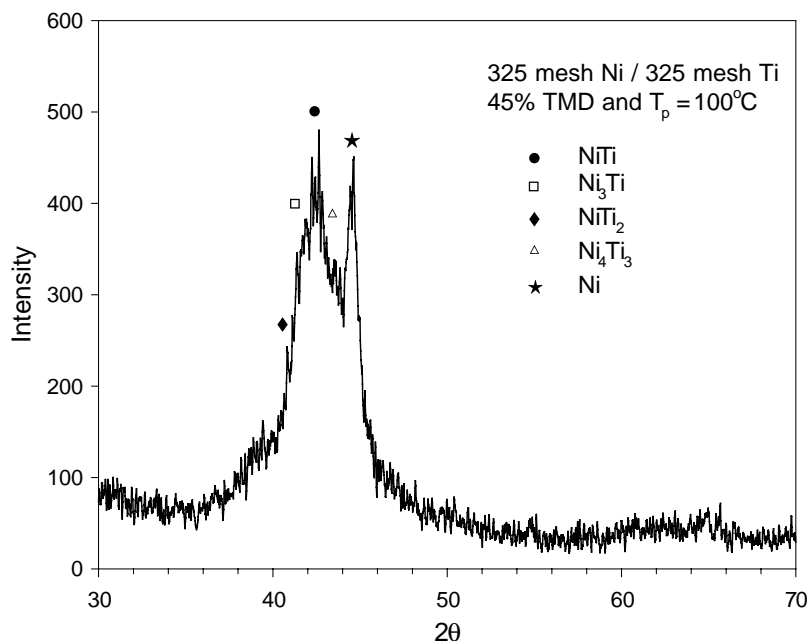


Fig. 14. XRD spectrum of product obtained from a 45% TMD sample compact using 325 mesh Ni powders at $T_p = 100^\circ\text{C}$.

relative density of the NiTi intermetallic was obtained from the sample using Ni powders of $3\text{--}7\ \mu\text{m}$ under $T_p = 300^\circ\text{C}$. SEM micrographs presented in Fig. 11(a) and (b) clearly indicate the difference in the microstructures of high-density and porous combustion products, respectively.

The XRD spectrum of the combustion product obtained from a 60% TMD sample with 325 mesh ($<45\ \mu\text{m}$) Ni powders at $T_p = 250^\circ\text{C}$ is shown in Fig. 12. It is apparent that the NiTi is the dominant phase in the end product due to the equiatomic Ni/Ti composition, while another stable phase Ni_3Ti and unreacted Ni are also observed in Fig. 12. When starting with the smaller Ni powders ($3\text{--}7\ \mu\text{m}$), the XRD analysis of the final product shown in Fig. 13 indicates an increase in the amount of NiTi phase. In addition, Fig. 13 also shows the presence of the other two secondary phases of NiTi_2 and Ni_3Ti . It is useful to note that the unreacted Ni was absent in Fig. 13. This implies that the use of finer Ni powders enhances the formation of NiTi intermetallic phase, which is consistent with the observation reported by Locci et al. [9].

The XRD spectrum of the porous product obtained from a 45% TMD sample under $T_p = 100^\circ\text{C}$ is shown in Fig. 14. Compared to those shown in Figs. 12 and 13, the amount of NiTi phase decreases and the quantity of unreacted Ni increases substantially in Fig. 14. Besides NiTi, NiTi_2 , and Ni_3Ti , the presence of a metastable phase Ni_4Ti_3 was observed in Fig. 14. This was believed to be caused by the lack of the prolonged second combustion stage for this sample, resulting in relatively short synthesis time and hence an incomplete reaction.

4. Conclusions

This study presents a comprehensive description of the SHS process associated with the formation of NiTi intermetallic compounds from elemental powder compacts. It was found that not only the product composition and morphology, but also the combustion characteristics are strongly affected by the initial sample density, preheating temperature, and reactant particle size.

For the sample compact with an initial density equal to or above 50% TMD, two consecutive combustion stages were observed during the synthesis process. The first combustion stage corresponds to the propagation of the flame-front. The second stage represents prolonged bulk combustion. Moreover, the propagation of flame-front during the first combustion stage is accompanied by a significant melting of the sample, resulting in the formation of high-density end products. For the 45% TMD samples under preheating temperatures of 100 and 150°C , the reaction process shows only the flame-propagation stage and almost no melting of the sample, due to the fact that the combustion temperature is lower than the lowest eutectic temperature of the Ni/Ti mixture. As a result, porous end products were obtained.

Based upon the measured combustion temperature, the significant melting of the sample was explained by the formation of the eutectic liquid phase. In addition, the combustion temperature was increased by increasing either the sample density or the preheating temperature. The self-sustained flame-front propagated in a steady mode and the propagation velocity increased significantly with the preheating temperature.

The XRD analysis indicates that the porous final product consists of a large amount of unreacted Ni, as well as several intermetallic phases including NiTi, NiTi₂, Ni₃Ti, and Ni₄Ti₃. However, the amount of unreacted Ni was greatly decreased and the amount of dominant compound NiTi was substantially increased in the dense products. The decrease of Ni particle size from 325 mesh (<45 μm) to 3–7 μm in the sample compacts further increased both the density of final products and the amount of NiTi phase. Moreover, the unreacted Ni was absent in the final composition when finer Ni powders were used. Besides the dominant phase NiTi, the other two stable phases of NiTi₂ and Ni₃Ti were also found in the products when Ni powders of 3–7 μm were used.

Acknowledgements

This research was sponsored by the National Science Council of Taiwan, R.O.C., under the grant of NSC 92-2212-E-212-015.

References

- [1] K. Otsuka, X. Ren, *Intermetallics* 7 (1999) 511–528.
- [2] H. Funakubo, *Shape memory alloys*, Gordon & Breach, New York, 1987.
- [3] Y. Liu, J.V. Humbeeck, R. Stalmans, L. Delaey, *J. Alloys Comp.* 247 (1997) 115–121.
- [4] D. Starosvetsky, I. Gotman, *Biomaterials* 22 (2001) 1853–1859.
- [5] A. Kapanen, J. Ryhänen, A. Danilov, J. Tuukkanen, *Biomaterials* 22 (2001) 2475–2480.
- [6] B.Y. Li, L.J. Rong, Y.Y. Li, V.E. Gjunter, *Acta Materialia* 48 (2000) 3895–3904.
- [7] Y.H. Li, L.J. Rong, Y.Y. Li, *J. Alloys Comp.* 345 (2002) 271–274.
- [8] M. Bram, A. Ahmad-Khanlou, A. Heckmann, B. Fuchs, H.P. Buchkremer, D. Stöver, *Mater. Sci. Eng. A* 337 (2002) 254–263.
- [9] A.M. Locci, R. Orrù, G. Cao, Z.A. Munir, *Intermetallics* 11 (2003) 555–571.
- [10] A.G. Merzhanov, *Ceram. Int.* 21 (1995) 371–379.
- [11] J.J. Moore, H.J. Feng, *Prog. Mater. Sci.* 39 (1995) 243–273.
- [12] H.C. Yi, J.J. Moore, *J. Mater. Sci.* 24 (1989) 3449–3455.
- [13] H.C. Yi, J.J. Moore, *J. Mater. Sci.* 24 (1989) 3456–3462.
- [14] S.H. Lee, J.H. Lee, Y.H. Lee, D.H. Shin, Y.S. Kim, *Mater. Sci. Eng. A* 281 (2000) 275–285.